Optimal Control of Electrical Interfaces for Triboelectric Kinetic Energy Harvesters Powering Low-Voltage Loads

Armine Karami, Philippe Basset, Dimitri Galayko

OPTIMAL CONTROL OF ELECTRICAL INTERFACES FOR TRIBOELECTRIC KINETIC ENERGY HARVESTERS POWERING LOW-VOLTAGE LOADS

Armine Karami[1], Philippe Basset[1], and Dimitri Galayko[2]
[1]Univ Gustave Eiffel, CNRS, ESYCOM, F-77454 Marne-la-Vallée, France and
[2]Sorbonne Université, CNRS, LIP6, F-75005 Paris, France

ABSTRACT
Kinetic energy harvesters based on triboelectric nanogenerators (TENGs) typically have output voltages in the range of few hundreds to few thousands of volts. This voltage should be controlled by the conditioning circuit to maximize power conversion. In addition, the conditioning circuit must provide the converted energy to the electrical load at a regulated low voltage. In this paper, we present a buck-like interface controlled to ensure proper low-voltage regulation at the load, while maximizing converted power. The control is based on the mechanical operating conditions and on the transducer characteristics. Experimental results validate the maximum power points predicted from charge-pump theory and illustrate the operation of the energy-extracting circuit. The results highlight the impact of the non-idealities of this circuit.

KEYWORDS
Kinetic energy harvesting, triboelectric nanogenerators, power management, charge-pumps, maximum power-point tracking

INTRODUCTION

Triboelectric nanogenerators (TENGs) are electrostatic transducers used for harvesting kinetic energy from vibrations, body motion, water waves, or wind flow [1-3]. Such systems aim at supplying autonomous embedded systems, in replacement or in complement of a battery. The size of TENG-based energy harvesters typically ranges from a few cm^3 to a few tens of cm^3. These transducers couple the principles of contact electrification and electrostatic induction through the transducer's capacitance variation [4]. Upon physical contact between two materials of different electron attraction abilities (dielectric-dielectric, or dielectric-conductor), charges will be trapped inside at least one of the dielectric layers. Opposite charges are therefore induced on the surfaces of the two transducer's electrodes. When the transducer capacitance varies due to external mechanical forces, a current flows between its electrodes through the connected conditioning circuit.

In open-circuit configuration, the voltage output of contact-separation or sliding-mode TENGs are high-voltage AC waveforms, typically ranging from a few tens of volt to several kilovolt in amplitude. Therefore, the conditioning circuit should at least serve as a rectifier. Besides, the electromechanical power converted by a TENG is directly related to the dynamics of the voltage set by this electrical conditioning circuit.

Charge-pumps are a specific class of conditioning circuits for TENGs. They have the major advantage of not needing an active synchronization with the external mechanical input [5]. Charge-pumps in turn divide into unstable and stable charge-pumps. Among the latter subclass, the half-wave (HW) rectifier has often been used as the conditioning circuits for TENGs [6].

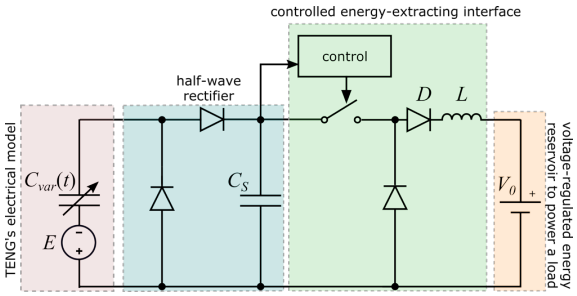

Figure 1: Sketch of the complete TENG-based kinetic energy harvesting system considered in this paper. The different parts are highlighted: the electrical lumped-model of the TENG, the half-wave conditioning circuit, and the energy-extracting interface.

Charge-pump conditioning circuits are often employed alone by directly connecting their output capacitor to the electrical load. But this direct energy transfer is not optimal. This is because of the large difference between the optimal charge-pump output voltage for maximum power conversion (typically a few hundred volts), and the electrical load supply requirements (typically a few volts). Therefore, an energy-extracting interface is needed to control the charge-pump. It is responsible for (i) keeping the charge-pump in a maximum power conversion state, while (ii) supplying the converted power to the electrical load at a suitable voltage.

This interface is a DC-DC converter controlled by a switch. The switch control is asynchronous with respect to the mechanical dynamics, hence keeping the auto-synchronicity advantage of charge-pumps. In addition to the components of the HW rectifier and of the energy-extracting circuit, the converted power made available to the load depends on the switch control policy. Some TENG-based electrostatic kinetic energy harvesters with this type of interface have been reported [7-9].

Most of these works focused on the task of rectification and stepping down of the TENG output voltage ((ii) above). The explicit quantification and maximization of the resulting converted power ((i) above), is often not considered. This requires studying the coupling between the charge-pump dynamics and the energy-extracting circuit operation. Most state-of-the-art works consider the two stages separately

In this paper, we study the optimal operation of the half-wave rectifier controlled by the energy-extracting interface. We first recall the TENG and half-wave electrical models, and their autonomous dynamics. Based on these dynamics, the key figures of converted power are

derived. The energy-extracting interface is then described, and experimental results validate the converted power quantities derived in the first part. Finally, the converted power at the output of the energy-extracting interface is measured and discussed.

CHARGE-PUMP DYNAMICS AND POWER

The electrical lumped model that we use for the TENG transducer is depicted in the leftmost part of Figure 1 [4]. The half-wave rectifier charge-pump (HW) connected to the transducer is also depicted in this figure. We suppose that the TENG's capacitance $C_{var}(t)$ is varying periodically between local maxima of value C_{max} and local minima of value C_{min}, with period $T = 1/f$. We define $\eta = C_{max}/C_{min}$. The DC source of value E models the effect of the charges trapped in the dielectric(s) upon contact. Its value depends on multiple parameters, such as the contact characteristics [10], but also environmental conditions [11].

Stable charge-pumps dynamics driven by C_{var} variation from discharged initial state are governed by

$$V_n = \beta(1 - \alpha^n) \qquad (1)$$

where V_n denotes the voltage across the output capacitor (C_S) at cycle n of C_{var}'s variation, when $C_{var} = C_{max}$. The values of $0 < \alpha < 1$ and $\beta > 0$ are determined as a function of the charge-pump topology, E, C_{max}, C_{min}, and the circuit's fixed capacitances. For the HW charge pump considered in this paper, we have

$$\alpha = \frac{C_S}{C_{min} + C_S}$$

and, for the saturation voltage β (reached upon autonomous operation across C_S as $n \to +\infty$)

$$\beta = E(\eta - 1).$$

The energy converted at cycle n is simply

$$\Delta W_n = C_S(1 - \alpha)(2\alpha V_n - (1 + \alpha)V_n^2 - (1 - \alpha)\beta^2)$$

These expressions are obtained considering an ideal, zero-threshold voltage diode model.

In the following, we suppose that $C_S \gg C_{min}$. Since C_S is a design parameter, this assumption constrains the range of obtainable dynamics. However, all key figures of converted power are increasing functions of C_S. Still, a small C_S can be useful in some applications where maximizing the converted power is not the main objective, but where a fast voltage increase is sought instead.

Under the $C_S \gg C_{min}$ assumption, the increment in voltage from cycle n to $n + 1$ is small in virtue of (1), and therefore the voltage evolution can be considered as continuous. We may substitute V_n with V $(0 < V < \beta)$ in (4) and seek the voltage at which the converted energy per cycle – now the instantaneous converted power – is maximum. Using $C_S \gg C_{min}$, this voltage is found to be $V^* = \beta/2$. The maximum instantaneous power is

$$P^* = fC_{min}\beta^2/4.$$

Another figure of converted power that is relevant is the maximum average converted power from initial state $V_n = 0$, or average converted power from zero. The average converted power from zero reads, at cycle n of C_{var}'s variation:

$$\bar{P}_n = \frac{fV_n^2 C_S}{2n}$$

The cycle n^* at which it is maximum is readily found:

$$\frac{\partial \bar{P}_n}{\partial n}(n^*) = 0 \;\Leftrightarrow\; \alpha^{n^*}(1 - 2n^* \log(\alpha)) = 1$$

whose solution is of the form $n^* = c/\log(\alpha)$, where c must verify $(1 - 2c)e^c = 1$, of which the solution is $c = 1/2 + \mathcal{W}_{-1}(-e^{-1/2}/2\,) \approx -1.26$. So, in all

$$n^* = \frac{1.26}{\log(\alpha^{-1})}.$$

The corresponding voltage across C_S is

$$\bar{V}^* = \beta(1 - e^{-1.26}) \approx 0.716\beta,$$

and

$$\bar{P}^* \approx 0.2fC_S\beta^2 \log(\alpha^{-1}) \approx 0.2fC_{min}\beta^2 = \frac{4}{5}P^*.$$

Both maximum converted power P^* and average converted power from zero $\bar{P}^*$ can be supplied into a useful load, thanks to a buck converter extracting energy from the

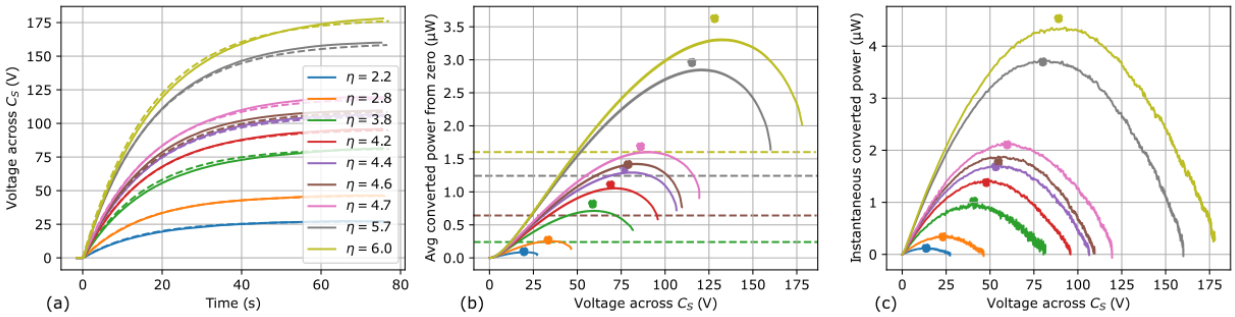

Figure 2: (a) Voltage evolution across the HW output capacitor C_S for different mechanical forcings, and hence different values of η. Model (dashed) and experimental (plain). (b) Measured average converted power from zero versus voltage across C_S. The position of each dot corresponds to (V^*, P^*) as predicted by the model. The dashed lines indicate the level of average converted power obtained at the output of the energy-extracting interface (c) Measured instantaneous converted power. The position of each dot corresponds to $(\bar{V}^*, \bar{P}^*)$ as predicted by the model.

charge-pump. The description of this circuit follows.

VOLTAGE DOWN-CONVERSION AND MPPT

Typical values of the triboelectric built-in voltage E range from tens to hundreds of volts, depending on the device geometry, the dielectric layer material, and the contact conditions. This is therefore also the case of the maximum instantaneous power voltage V^*. In contrast, the nominal voltage of many useful electrical load is at least an order of magnitude lower. If a load is directly connected to the HW output capacitor, its voltage requirements force the transducer + charge-pump system to operate sub-optimally, possibly drastically off from the maximum achievable instantaneous power.

To overcome this possible shortfall in converted and supplied power, we propose an energy-extracting interface, depicted in the rightmost part of Figure 1. This interface has the topology of a buck converter. It controls the charge-pump state asynchronously with respect to the mechanical input forcing. This circuits extracts energy at high-voltage from C_S into a low-voltage reservoir, with power close to the maximum achievable by the transducer + charge-pump system. In the following, we suppose that the load's voltage is regulated by another circuit to some average value V_0.

This interface operates as follows: when $V_S = V_X$ where V_X is some predetermined voltage, the switch is closed. The electrostatic energy accumulated in C_S from kinetic-to-electric energy conversion is transferred to both the source V_0, and to the inductor L, as the magnetic field builds up through it. Thanks to the diode D, the energy is prevented from bouncing back into C_S (needed if the switch cannot be controlled accurately enough). Then, when the switch is opened, the inductor demagnetizes, and its energy is transferred to the source V_0. The net result of the total process is that the energy removed from C_S is supplied to V_0, short of a dissipated amount.

The control policy of the switch is set by the (possibly dynamic) choice of the voltage V_X, and the condition for switch opening. For example, to sustain the maximum instantaneous power P^*, one should choose $V_X = V^*$. Furthermore, the switch should be opened after a small fraction of $\tau = 2\pi\sqrt{LC_S}$. If τ is too small, the control can be challenging to achieve, depending on the switch implementation. Sustaining the maximum average power from zero $\bar{P}^*$ at the load requires less accuracy in terms of switch control, as the switch should discharge C_S completely when $V_X = \bar{V}^*$. However, compared with the maximum instantaneous power policy (i) the maximum achievable power is 20% less ($\bar{P}^* = 0.8P^*$), and (ii) the voltage ripple is larger under steady mechanical forcing.

In the following experiments, we use an externally actuated relay. Given its limited control accuracy, we implement the maximum average power from zero switch control. Better implementations of the switch can be based on, e.g., MOSFET transistors [8]. But their control is challenging at high voltages (few hundred volts) *and* low power. This is why other technological solutions have emerged, e.g., self-powered MEMS plasma switches [12].

RESULTS

Experiments were carried out to validate the HW dynamics, and the figures of maximum converted power. The transducer consists in two 4.5×4.5 cm^2 plastic plates, whose facing sides are covered with aluminum tape. One of the two tapes is covered with a dielectric layer of PTFE (polytetrafluoroethylene) of average thickness 30 µm. An open-loop linear motor (Modalshop K2007E) driven by a function generator is used to apply the periodic mechanical forcing to the transducer, normally to the electrodes plane. Electrically, two different configurations are used. First, the transducer can be connected to the HW rectifier, with a high-voltage C0G output capacitor of value $C_S = 9.8$ nF. The voltage across this capacitor is found by time-integration of the current flowing through it. This current is measured through a SRS570 low-noise current preamplifier. The diodes in the charge-pump conditioning circuit are MMBD1503A-D87Z. The second electrical configuration of the transducer is used to dynamically measure its capacitance variation $C_{var}(t)$, by a method that is essentially the same as in [13] for MEMS transducers.

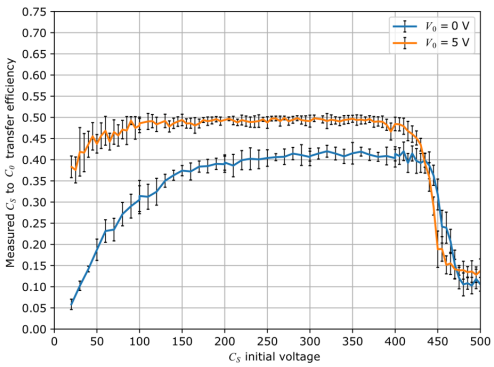

Figure 3: Efficiency of the energy transfer from the charge-pump output capacitor C_S to the output capacitor C_0, versus initial voltage across C_S and for two values of the initial voltage across C_0.

The transducer was tested in both configurations for a range of 9 different mechanical forcing amplitudes. From the dynamic capacitance measurement configuration, the average values of η corresponding to each forcing (10 measurements per forcing) are listed in the legend of Figure 2a. The values of η increase with increasing forcing. While C_{min} remains constant, dominated by a parasitic capacitance, C_{max} increases by increasing the forcing, due to a small relative deformation of the dielectric layer.

For each forcing, the transducer was also tested with the HW rectifier in autonomous operation. The results in terms of the voltage across C_S are depicted in Figure 2a. From this voltage evolution, the average converted power from zero and the instantaneous converted power are computed and plotted in Figure 2b and 2c, respectively. These figures also show plots of the theoretical evolution predicted by model (1), and the loci of maximum power quantities. It is important to note that the value of E was adjusted for each forcing. Indeed, E and the forcing amplitude are not independent, and thus E and η are not independent across the range of the 9 forcings. This is because increasing the forcing also has the effect of increasing the effective contact area, hence the trapped charge at constant nominal contact area, and hence the

voltage E, up to a saturation level [14]. With this fitting procedure, the model and measurements closely match, and validate the mathematical form of the model (1) up to a multiplicative constant. The measurement also supports the models of converted power figures and associated V_S voltages. The mismatch is due to (i) propagation of the uncertainty in the measurement of C_{min} (measured averages are used for the plots) to η, the model (1), and to the expressions of converted power, and to (ii) losses in the diodes (leakage increasing with V_S, forward voltage drop).

We then tested the energy-extracting interface actuated with the $V_X = \bar{V}^*$ control policy, for a few different forcings. The circuit consists in a 18 mH inductor of measured $DCR = 29.1\ \Omega$ (RFC1010B-186KE). The diodes used in the interface are Vishay BYW55 diodes. The switch is a IMB03CGR mechanical relay, actuated by a signal from an external source. We implement the source V_0 with a capacitor $C_0 = 1$ µF, initially charged at $V_0 = 5$ V . The average output power across C_0 was measured, after 10 actuations occurring at $V_S = \bar{V}^*$. We find that the average power corresponds to the maximum average power from zero at the load output divided by a factor of about 2, as shown in Figure 2b (dashed line levels). To understand these results, we separately measured the efficiency of the energy-extracting interface, with results depicted in Figure 3. In this plot, each point is obtained by averaging 10 measurements of the efficiency. The error bars height is of 1 standard deviation. We find an efficiency of about 50%, explaining the factor 2 in the power measurements with the energy-extracting interface. A major reason for the relatively low efficiency is the uncontrolled bouncing of the mechanical relay at closing. For comparison, a SPICE simulation of the same circuit with accurate BYW55 diode model but ideal switch yields an efficiency of 70% to 75% in the considered voltage range.

These results and the discussion in the end of the previous section show that, in general, the choice of the control policy and the sizing of the energy-extracting interface must be done in a holistic way. This choice is the result of an optimization procedure that should simultaneously consider, at least, dissipation sources in the extraction circuit, maximum voltage constraints, practical control accuracy, and mechanical input conditions.

CONCLUSION

Kinetic energy harvesters based on TENGs are often electrically conditioned by a half-wave rectifier. An energy-extracting interface is needed at the output of this rectifier to ensure optimal power conversion by the TENG while satisfying load voltage requirements. A circuit was presented to fulfill this role. We derived the maximum power points achievable at the output of this circuit. Experimental results support the system model and highlight the impact of power dissipation in the interface. This leaves room for further improvement, by both technological (e.g., switch implementation) and system-level optimization (control strategy, components sizing).

CONTACT

*A. Karami, armine.karami@univ-eiffel.fr

REFERENCES

[1] C. Zhang, L. He, L. Zhou et al., "Active resonance triboelectric nanogenerator for harvesting omnidirectional water-wave energy," *Joule* vol. 5 (6), pp. 1613-1623 (2021).

[2] W. Li, Y. Liu, S. Wang et al., "Vibrational Triboelectric Nanogenerator-Based Multinode Self-Powered Sensor Network for Machine Fault Detection," *IEEE/ASME Transactions on Mechatronics* vol. 25 (5), pp. 2188-2196 (2020).

[3] D. Jiang, G. Liu, W. Li et al., "A Leaf-Shaped Triboelectric Nanogenerator for Multiple Ambient Mechanical Energy Harvesting," *IEEE Transactions on Power Electronics* vol. 35 (1), pp. 25-32 (2020).

[4] R. Hinchet, A. Ghaffarinejad, Y. Lu et al., "Understanding and modeling of triboelectric-electret nanogenerator," *Nano Energy* vol. 47, pp. 401-409 (2018).

[5] D. Galayko, A. Dudka, A. Karami et al., "Capacitive Energy Conversion With Circuits Implementing a Rectangular Charge-Voltage Cycle—Part 1: Analysis of the Electrical Domain," *IEEE Transactions on Circuits and Systems I: Regular Papers* vol. 62 (11), pp. 2652-2663 (2015).

[6] A. Ghaffarinejad, J. Yavand Hasani, D. Galayko et al., "Superior performance of half-wave to full-wave rectifier as a power conditioning circuit for triboelectric nanogenerators: Application to contact-separation and sliding mode TENG," *Nano Energy* vol. 66, pp. 104137 (2019).

[7] W. Harmon, D. Bamgboje, H. Guo et al., "Self-driven power management system for triboelectric nanogenerators," *Nano Energy* vol. 71, pp. 104642 (2020).

[8] F. Xi, Y. Pang, W. Li et al., "Universal power management strategy for triboelectric nanogenerator," *Nano Energy* vol. 37, pp. 168-176 (2017).

[9] J. Maeng, I. Park, M. Shim et al., "A High-Voltage Dual-Input Buck Converter With Bidirectional Inductor Current for Triboelectric Energy-Harvesting Applications," *IEEE Journal of Solid-State Circuits* vol. 56 (2), pp. 541-553 (2021).

[10] G. Min, Y. Xu, P. Cochran et al., "Origin of the contact force-dependent response of triboelectric nanogenerators," *Nano Energy* vol. 83, pp. 105829 (2021).

[11] V. Nguyen and R. Yang, "Effect of humidity and pressure on the triboelectric nanogenerator," *Nano Energy* vol. 2 (5), pp. 604-608 (2013).

[12] H. Zhang, F. Marty, X. Xia et al., "Employing a MEMS plasma switch for conditioning high-voltage kinetic energy harvesters," *Nat Commun* vol. 11 (1), pp. 3221 (2020).

[13] P. Basset, D. Galayko, A. M. Paracha et al., "A batch-fabricated and electret-free silicon electrostatic vibration energy harvester," *Journal of Micromechanics and Microengineering* vol. 19 (11), pp. 115025 (2009).

[14] Y. Xu, G. Min, N. Gadegaard et al., "A unified contact force-dependent model for triboelectric nanogenerators accounting for surface roughness," *Nano Energy* vol. 76, pp. 105067 (2020).